

Terahertz-field-driven metastable topological phase in an atomically thin crystal

Authors: Jiaojian Shi^{1†}, Ya-Qing Bie^{2,3†*}, Wei Chen⁴, Shiang Fang^{4,5}, Alfred Zong^{2,6}, Jinchi Han⁷, Zhaolong Cao³, Yong Zhang⁸, Takashi Taniguchi⁹, Kenji Watanabe¹⁰, Vladimir Bulović⁷, Efthimios Kaxiras⁴, Pablo Jarillo-Herrero^{2*}, Edoardo Baldini^{11*}, Keith A. Nelson^{1*}.

Affiliations:

¹Department of Chemistry, Massachusetts Institute of Technology, Cambridge, MA 02139, USA.

²Department of Physics, Massachusetts Institute of Technology, Cambridge, MA 02139, USA.

³State Key Lab of Optoelectronic Materials and Technologies, Guangdong Province Key Laboratory of Display Material and Technology, School of Electronics and Information Technology, Sun Yat-sen University, Guangzhou, 510275, People's Republic of China.

⁴Department of Physics, Harvard University, Cambridge, MA 02138, USA.

⁵Department of Physics and Astronomy, Center for Materials Theory, Rutgers University, Piscataway, NJ 08854, USA.

⁶Department of Chemistry, University of California, Berkeley, CA 94720, USA.

⁷Department of Electrical Engineering and Computer Science, Massachusetts Institute of Technology, Cambridge, MA 02139, USA.

⁸Center for Materials Science & Engineering, Massachusetts Institute of Technology, Cambridge, MA 02139, USA.

⁹International Center for Materials Nanoarchitectonics, National Institute for Materials Science, 1-1 Namiki, Tsukuba 305-0044, Japan.

¹⁰Research Center for Functional Materials, National Institute for Materials Science, 1-1 Namiki, Tsukuba 305-0044, Japan.

¹¹Department of Physics, Center for Complex Quantum System, The University of Texas at Austin, Austin, TX 78712, USA.

*Correspondence to: Y.-Q.B. (bieyq@mail.sysu.edu.cn), P.J.-H. (pjarillo@mit.edu), E.B. (edoardo.baldini@austin.utexas.edu), K.A.N. (kanelson@mit.edu)

†These authors contributed equally.

Abstract: Light-induced topological phase transitions in quantum materials are notoriously difficult to realize and can persist only for ultrashort timescales in dissipative environments. Stabilizing a metastable topological phase indefinitely with light thus remains a grand challenge in condensed matter physics. Here, we achieve this goal by irradiating the atomically thin transition metal dichalcogenide MoTe₂ with tailored field-enhanced terahertz (THz) pulses. The THz-field induced topological phase transition proceeds through a structural transformation from the trivial hexagonal (*2H*) to the topological insulator distorted (*1T'*) phase, leading to a metastable state that persists indefinitely over months after THz exposure. To characterize the metastable phase and map its formation dynamics, we use a suite of advanced spectroscopic and diffraction probes.

Corroborated with frequency-dependent measurements, they verify the uniqueness of THz excitation in driving the transition. State-of-the-art *ab initio* calculations further clarify the complex interplay of electronic and ionic degrees of freedom at the origin of the THz-field-induced transformation. Our results open up an avenue in the generation and detection of topological states that may not have a counterpart in thermodynamic equilibrium.

Main Text:

Metastability is a ubiquitous concept in physics and chemistry, governing phenomena as diverse as the radioactive decay of nuclear isomers and the superheating dynamics of liquid-gas mixtures (1, 2). In condensed matter systems, metastability often plays a crucial role in crystallographic polymorphism and thus provides a promising avenue for control over structure-function relationships in materials. However, finding novel metastable states with exotic functionalities requires systematic scrutiny of candidate material systems, as well as an accurate choice of external stimuli. In recent years, ultrashort light pulses have shown great potential to induce metastable states in quantum materials by breaking the subtle balance among different microscopic degrees of freedom. Solids that are particularly prone to undergo nonequilibrium transformations into hidden metastable phases are those with strong electronic correlations, as their complex potential energy landscapes depend on the intricate interplay of the charge, spin, orbital, and lattice subsystems (3, 4). However, the realization of *topologically* non-trivial metastable states induced by light remains still unexplored. Achieving this long-sought goal would open new paradigms in the study of nonequilibrium quantum materials and pave the way for applications where light manipulates band topology beyond the transient ultrashort timescale (5-9).

Here, we demonstrate the first light-induced metastable topological phase that lasts over months without noticeable recovery. We initiate this topological phase transition by irradiating an atomically thin crystal with high-field terahertz pulses, and visualize the resulting metastable state through a suite of spectroscopic and diffraction probes. The implementation of THz excitation is motivated by the far-from-equilibrium electronic and ionic excursions driven by the THz electric field, with negligible heating effects. The material system in question is $2H\text{-MoTe}_2$, a transition metal dichalcogenide that crystallizes in a non-centrosymmetric hexagonal unit cell. It is composed of a layer of hexagonally arranged transition metal atoms, sandwiched between two layers of chalcogen atoms (Fig. 1A). Its electronic structure -- shown in Fig. 1B (see the Methods section for computational details) -- exhibits a direct gap of the order of 1 eV along the Γ -S direction of the Brillouin zone (10), and the material is topologically trivial. The transition to the centrosymmetric $1T'$ phase proceeds through a Peierls distortion along the y -axis, with the transition metal atoms octahedrally coordinated to the surrounding chalcogen atoms (11) (Fig. 1C). This structural distortion leads to a significant electronic structure reconstruction involving band inversion around the Γ point. A hole-like band at Γ and an electron-like band appear close to the Fermi energy, crossing each other at a point along the Γ -X line. For thin enough samples (up to 10 layers), the presence of spin-orbit coupling lifts the degeneracy at the crossing point, opening a narrow gap of ~ 60 meV (11) (Fig. 1D). The interplay between the inverted band structure and spin-orbit coupling-induced gap drives few-layered $1T'$ - MoTe_2 into a quantum spin Hall insulator state (12). The non-trivial topological character of this polymorph can be assessed through a Fu-Kane parity analysis of the associated Z_2 topological index (as shown in Fig. 1D) (13, 14).

In our experiments, we positioned a flake of h-BN-encapsulated $2H$ -MoTe₂ on top of two parallel gold strips separated by a gap (Fig. 2A). Upon illumination of this structure with a free-space THz pulse, the field strength was enhanced by a factor of about 20 inside the gap, reaching amplitudes as large as several MV/cm (see Methods) (15). The h-BN layers isolated $2H$ -MoTe₂ from possible field-induced charge emission from the gold layers (16) and prevented its direct exposure to air. Figure 2B shows the optical image of a monolayer sample that we prepared using a dry transfer method (17). After irradiating this structure with a free-space THz field of 270 kV/cm, we probed possible changes in the lattice via spontaneous Raman scattering. Figure 2C shows the Raman spectrum before THz illumination. It comprises the A_{1g} phonon at 171.5 cm⁻¹ and the E_{2g} phonon at 236 cm⁻¹, in agreement with previous studies of the $2H$ phase (11). After excitation with five THz pulses, both modes of the $2H$ phase disappear and a peak at 163.3 cm⁻¹ emerges. This feature is a specific fingerprint of the $1T'$ phase of MoTe₂ (11), and its presence suggests a change of crystalline symmetry. The new phonon peak becomes more prominent with further THz exposure, indicating the growth of a larger $1T'$ sample area. The spectrum does not show any localized modes due to damage-related Te clusters (18). Thus, already at this stage, we could conclude that the action of THz field on our monolayer MoTe₂ is to induce a phase transition from the topologically trivial $2H$ to the non-trivial $1T'$ polymorph.

To further investigate this phase transformation, we conducted more detailed experiments. Since the induced $1T'$ phase is long-lived, each measurement required a fresh sample, carefully positioned over an insulating gap as indicated above. First, we studied how the $2H$ phase responded to a sequence of THz pulses with gradually increasing field strengths. To probe the phase transition, we tracked the changes in crystalline symmetry via optical second harmonic generation (SHG), a sensitive probe of inversion symmetry breaking that can distinguish between the topologically trivial $2H$ phase (non-centrosymmetric) and the topologically non-trivial $1T'$ phase (centrosymmetric). Figure 3A shows three representative images of the SHG intensity prior to irradiation and following THz-field exposure with free-space amplitudes of 183 kV/cm and 240 kV/cm. A plot of the SHG intensities from three sample locations within the field-enhancement gap (labeled I, II, III in Fig. 3A) is presented in Fig. 3B. We observe that the SHG signal drops when the field strength exceeds 183 kV/cm, disappearing completely above 270 kV/cm. As the field enhancement factor generated by the gold strips is ~ 20 , the threshold needed to quench the SHG intensity can be estimated to be around 4.0 MV/cm. We complemented these measurements by recording Raman spectra as a function of THz field strength. Figure 3C shows spectra acquired after irradiation at 200 kV/cm and 270 kV/cm. Consistent with the picture supported by the SHG results of Fig. 3B, irradiation at ~ 200 kV/cm leads to a first drop in the intensity of the $2H$ phonons and to their strong suppression above 270 kV/cm. Simultaneously, the Raman mode of the $1T'$ phase grows in, eventually dominating the spectrum after irradiation with 1000 pulses at 270 kV/cm. We also established the wide range of our findings by inducing the structural and topological phase transition in bi- and multi-layer (~ 10 layers) samples. Figures 3D and 3E show the results obtained on a multi-layer sample, presenting the [001] zone-axis electron diffraction pattern and Raman spectrum before and after irradiation with a single THz pulse at 300 kV/cm. We observe that the diffraction pattern of the unexcited crystal exhibits the 6-fold symmetry expected for the $2H$ phase. Consistent with this, the Raman spectrum displays only an E_{2g} phonon mode of bulk $2H$ -MoTe₂ (10). After THz irradiation, new peaks emerging in the diffraction pattern of the (001) plane (19-22) reveal a cell-doubling structure, accompanied by the appearance of the A_g Raman-active phonon (11). Both observables are characteristic signatures of the distorted $1T'$

phase. More details about the electron diffraction measurement can be found in Supplementary Note 3.

All the above results conclusively indicate the emergence of a THz field-induced topologically non-trivial metastable phase in $2H$ -MoTe₂ upon THz irradiation. The lifetime of this state is remarkably long, as the samples did not relax back to the $2H$ phase even after months (*i.e.* the time elapsed until the present writing) from THz exposure.

To gain microscopic insights into the THz-driven topological phase transition, we also explored its dynamics. This represents a challenging task for conventional time-resolved spectroscopy methods because their stroboscopic approach precludes the study of irreversible photoinduced processes. We therefore developed a specialized apparatus for THz pump-SHG probe single-shot spectroscopy, which is well suited for probing the formation dynamics of long-lived metastable states. A schematic illustration of our experiment is presented in Fig. 4A (see the Methods section for more details). In our measurements, we irradiated trilayer samples with a THz-field strength exceeding the phase transition threshold and we reconstructed the dynamics at different pump-probe delays. Since the THz field level was above the threshold for generating the $1T'$ phase, each shot with its predetermined delay time for the optical probe pulse was conducted on a different sample.

Figure 4B shows the time evolution of the SHG signal following THz excitation (blue dots). The response initially increases, reaching about twice the initial value (I_i) at 20 ps. It then remains higher than I_i for several hundred picoseconds, before dropping to $\sim 0.4I_i$ at 12.5 ns. Finally, the SHG signal disappears completely, indicating the stabilization of the $1T'$ phase. This is further confirmed by the measurement of the SHG intensity of each sample 1 minute after exposure, as shown by the red dots in Fig. 4B. We could verify these complex dynamics on different samples, with the initial enhancement of the SHG occurring even below the phase transition threshold. From our single-shot spectroscopy data, we could identify the characteristic timescale on the order of several nanoseconds to switch $2H$ -MoTe₂ into the $1T'$ polymorph. This timescale is comparable to the reported carrier recombination lifetimes in few-layer MoTe₂ (23). The increase in SHG observed at shorter times is also intriguing, but it requires further study to reach complete understanding. We believe it may be associated with the nucleation of a transient phase with lower crystalline symmetry, for example the distorted trigonal prismatic $2H^*$ phase (24, 25).

To rationalize our findings, we theoretically explored different effects that can lie at the origin of the $2H$ -to- $1T'$ topological phase transition. Based on the nanosecond phase transition dynamics, a natural hypothesis involves a THz-field driven carrier excitation mechanism. Microscopically, an intense electric field at THz frequency can generate high carrier densities through mechanisms such as the Poole-Frenkel ionization that liberate carriers and accelerate them to multi-eV energies. These processes lead to impact ionization, liberating more carriers and evolving as cascade events (26). In our experiments, carriers can remain as quasi-free in the bands or can localize at interfacial defects states, locally charging the sample (27). To account for both scenarios, we investigated the effect of a nonequilibrium (neutral) carrier distribution and of charge (*i.e.* electron) doping on the energetic landscape of MoTe₂. The results of our calculations are shown in Fig. 4C and 4D. At equilibrium, the metastable $1T'$ phase lies about 0.1 eV higher in energy than the $2H$ phase (blue horizontal lines). The activation barrier and reverse activation barrier are 1.66 eV and 1.56 eV, respectively, thus protecting the $2H$ and $1T'$ phases against thermal fluctuations. Upon excitation of a neutral electron-hole distribution (Fig. 4C) and charge doping (Fig. 4D), we find that the activation barrier lowers substantially (violet-to-red horizontal lines) and favors the occurrence of

the $2H$ -to- $1T'$ topological phase transition. Experimentally, we could establish that the excited electron-hole carriers have the leading role in the process. Indeed, we could estimate that the density of interface traps is three orders of magnitude smaller than the effective charge densities required to stimulate the phase transition (see Supplementary Note 4). We also investigated the role played by coherently driven phonons in favoring the structural transformation at faster timescales. Our normal-mode calculations show the existence of a low-energy vibrational mode that breaks the mirror symmetry of the two Te planes and can serve as a collective reaction coordinate connecting the $2H$ and $1T'$ phases (more details are given in Supplementary Note 6 and Fig. S19). This phonon mode is Raman active and can thus be driven coherently via a THz sum-frequency excitation process (28, 29), but this mechanism is unlikely to provide the driving force for the complex phase transition as it is second order in nature. Therefore, we believe that THz-induced changes in the carrier distribution are responsible for the MoTe_2 $2H$ -to- $1T'$ phase transition. We also performed experiments with mid-infrared and near-infrared pulsed excitation centered around 225 meV and 1.55 eV, respectively. We detected no changes in the original $2H$ crystal structure (Supplementary Fig. S13, S14), consistent with previous findings showing that excitation with high photon energies may induce defects in the form of Te clusters (18, 30-33). This indicates that THz excitation is the only pathway demonstrated so far for photoinduced generation of the $1T'$ phase, or any metastable topological phase, in MoTe_2 or any single-layer or few-layer transition metal dichalcogenides. This capability opens tantalizing perspectives in the search for novel phases of matter in other systems such as moiré heterostructures, where non-trivial band topology meets strong electronic correlations.

References:

1. K. Heyde, J. L. Wood, *Rev. Mod. Phys.* **83**, 1467-1521 (2011).
2. P. G. Debenedetti, *Metastable Liquids* (Princeton University Press, 1997).
3. J. Zhang, X. Tan, M. Liu, S. W. Teitelbaum, K. W. Post, F. Jin, K. A. Nelson, W. Wu, and R. D. Averitt, *Nat. Mater.* **15**, 956-960 (2016).
4. L. Stojchevska, I. Vaskivskiy, T. Mertelj, P. Kusar, D. Svetin, S. Brazovskii, D. Mihailovic, *Science* **344**, 177-180 (2014).
5. E. J. Sie, C. M. Nyby, C. D. Pemmaraju, S. J. Park, X. Shen, J. Yang, M. C. Hoffmann, B. K. Ofori-Okai, R. Li, A. H. Reid, *et al.*, *Nature* **565**, 61-66 (2019).
6. M. Y. Zhang, Z. X. Wang, Y. N. Li, L. Y. Shi., D. Wu, T. Lin, S. J. Zhang, Y. Q. Liu, Q. M. Liu, J. Wang, *et al.*, *Phys. Rev. X* **9**, 021036 (2019).
7. J. W. McIver, B. Schulte, F.-U. Stein, T. Matsuyama, G. Jotzu, G. Meier, A. Cavalleri, *Nat. Phys.* **16**, 38-41 (2020).
8. M. Budden, T. Gebert, M. Buzzi, G. Jotzu, T. Matsuyama, G. Meier, Y. Laplace, D. Pontiroli, M. Riccò, F. Schlawin, *et al.*, *Nat. Phys.* **17**, 611-618 (2021).
9. N. Yoshikawa, H. Suganuma, H. Matsuoka, Y. Tanaka, P. Hemme, M. Cazayous, Y. Gallais, M. Nakano, Y. Iwasa, R. Shimano, *Nat. Phys.* **17**, 909-914 (2021).
10. C. Ruppert, O. B. Aslan, T. F. Heinz, *Nano. Lett.* **14**, 6231-6236 (2014).
11. D. H. Keum, S. Cho, J. H. Kim, D.-H. Choe, H.-J. Sung, M. Kan, H. Kang, J.-Y. Hwang, S. W. Kim, H. Yang, *et al.*, *Nat. Phys.* **11**, 482-486 (2015).
12. X. Qian, J. Liu, L. Fu, J. Li, *Science* **346**, 1344-1347 (2014).
13. R. Yu, X. L. Qi, A. Bernevig, Z. Fang, X. Dai, *Phys. Rev. B* **84**, 075119 (2011).
14. L. Fu, C. L. Kane, *Phys. Rev. B* **76**, 045302 (2007).
15. B. C. Pein, W. Chang, H. Y. Hwang, J. Scherer, I. Coropceanu, X. Zhao, X. Zhang, V. Bulović, M.

- G. Bawendi, K. A. Nelson, *Nano Lett.* **17**, 5375-5380 (2017).
16. C. R. Dean, A. F. Young, I. Meric, C. Lee, L. Wang, S. Sorgenfrei, K. Watanabe, T. Taniguchi, P. Kim, K. L. Shepard, *et al.*, *Nat. Nanotechnol.* **5**, 722-726 (2010).
 17. L. Wang, I. Meric, P. Y. Huang, Q. Gao, H. Tran, T. Taniguchi, K. Watanabe, L. M. Campos, D. A. Muller, J. Guo, *et al.*, *Science* **342**, 614-617 (2013).
 18. S.-Y. Chen, C. H. Naylor, T. Goldstein, A. T. C. Johnson, J. Yan, *ACS Nano* **11**, 814-820 (2017).
 19. L. Wang, Z. Xu, W. Wang, X. Bai, *J. Am. Chem. Soc.* **136**, 6693-6697 (2014).
 20. P. Gao, L. Wang, Y. Zhang, Y. Huang, K. Liu, *ACS Nano* **9**, 11296-11301 (2015).
 21. J. Heising, M. G. Kanatzidis, *J. Am. Chem. Soc.* **121**, 11720-11732 (1999).
 22. L. Meng, Y. Ma, K. Shi, S. Xu, J. Wang, Y. Gong, *Tungsten* **1**, 46-58 (2019).
 23. K. Chen, A. Roy, A. Rai, H. C. P. Movva, X. Meng, F. He, S. K. Banerjee, Y. Wang, *APL Mater.* **6**, 056103 (2018).
 24. A. V. Kolobov, P. Fons, J. Tominaga, *Phys. Rev. B* **94**, 094114 (2016).
 25. F. Zhang, H. Zhang, S. Krylyuk, C. A. Milligan, Y. Zhu, D. Y. Zemlyanov, L. A. Bendersky, B. P. Burton, A. V. Davydov, J. Appenzeller, *Nat. Mater.* **18**, 55-61 (2019).
 26. K. Fan, H. Y. Hwang, M. Liu, A. C. Strikwerda, A. Sternbach, J. Zhang, X. Zhao, X. Zhang, K. A. Nelson, R. D. Averitt, *Phys. Rev. Lett.* **110**, 217404 (2013).
 27. L. Ju, J. V. Jr, E. Huang, S. Kahn, C. Nosiglia, H.-Z. Tsai, W. Yang, T. Taniguchi, K. Watanabe, Y. Zhang, *et al.*, *Nat. Nanotechnol.* **9**, 348-352 (2014).
 28. S. Maehrlein, A. Paarmann, M. Wolf, T. Kampfrath, *Phys. Rev. Lett.* **119**, 127402 (2017).
 29. D. M. Juraschek, S. F. Maehrlein, *Phys. Rev. B* **97**, 174302 (2018).
 30. S. Cho, S. Kim, J. H. Kim, J. Zhao, J. Seok, D. H. Keum, J. Baik, D.-H. Choe, K. J. Chang, K. Suenaga, *et al.*, *Science* **349**, 625-628 (2015).
 31. Y. Song, R. Tian, J. Yang, R. Yin, J. Zhao, X. Gan, *Adv. Opt. Mater.* **6**, 1701334 (2018).
 32. Y. Tan, F. Luo, M. Zhu, X. Xu, Y. Ye, B. Li, G. Wang, W. Luo, X. Zheng, N. Wu, *et al.*, *Nanoscale* **10**, 19964-19971 (2018).
 33. A. Krishnamoorthy, M.-F. Lin, X. Zhang, C. Weninger, R. Ma, A. Britz, C. S. Tiwary, V. Kochat, A. Apte, J. Yang, *et al.*, *Nano. Lett.* **19**, 4981-4989 (2019).

Acknowledgments: The authors acknowledge discussions and technical supports from Zefeng Ren, Xirui Wang, Yoseob Yoon, Brandt Pein, Pin-Chun Shen, Alexei Maznev, Tom Mahony, Frank Gao and Yu-Hsiang Chen. **Author contributions:** Y.-Q.B. and J.S. conceived the idea, conducted the experiments, and analyzed the data under guidance from P.J.-H. and K.A.N. W.C., S.F., and E.K. provided theoretical calculations. Y.-Q.B., J.H., and V.B. synthesized field enhancement structures. A.Z. and Y.Z. contributed to sample preparations and electron diffraction measurements. Z.C. performed the field enhancement calculations. T.T. and K.W. grew the crystals of hexagonal boron nitride. E.B., Y.-Q.B., and J.S. led the manuscript preparation. **Competing interests:** The authors declare having no competing financial interests. **Data and materials availability:** All data are available in the manuscript or the supplementary materials.

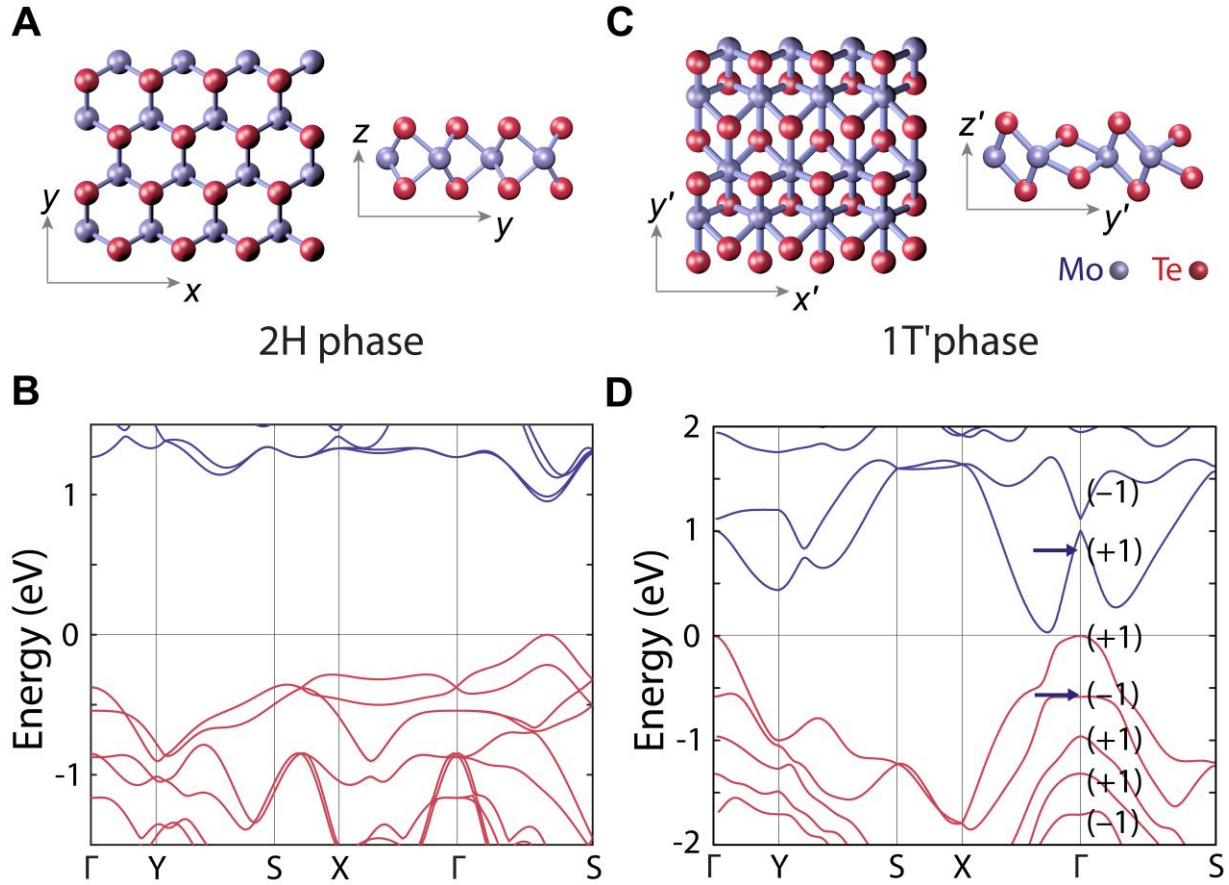


Fig. 1. Structurally-induced topological phase transition in MoTe₂. (A) The top and side view of the lattice structure of 2H MoTe₂. (B) The electronic band structure for the 2H monolayer MoTe₂. (C) The top and side view of the lattice structure of 1T' MoTe₂. (D) The electronic band structure for the 1T' monolayer MoTe₂ and Fu-Kane parity analysis of the associated Z_2 topological index. The inversion symmetry eigenvalues for bands near the Fermi level at Γ point are labeled. The topological index in black is computed with the filled bands. Figure adapted from: Ref. (11), Springer Nature Ltd.

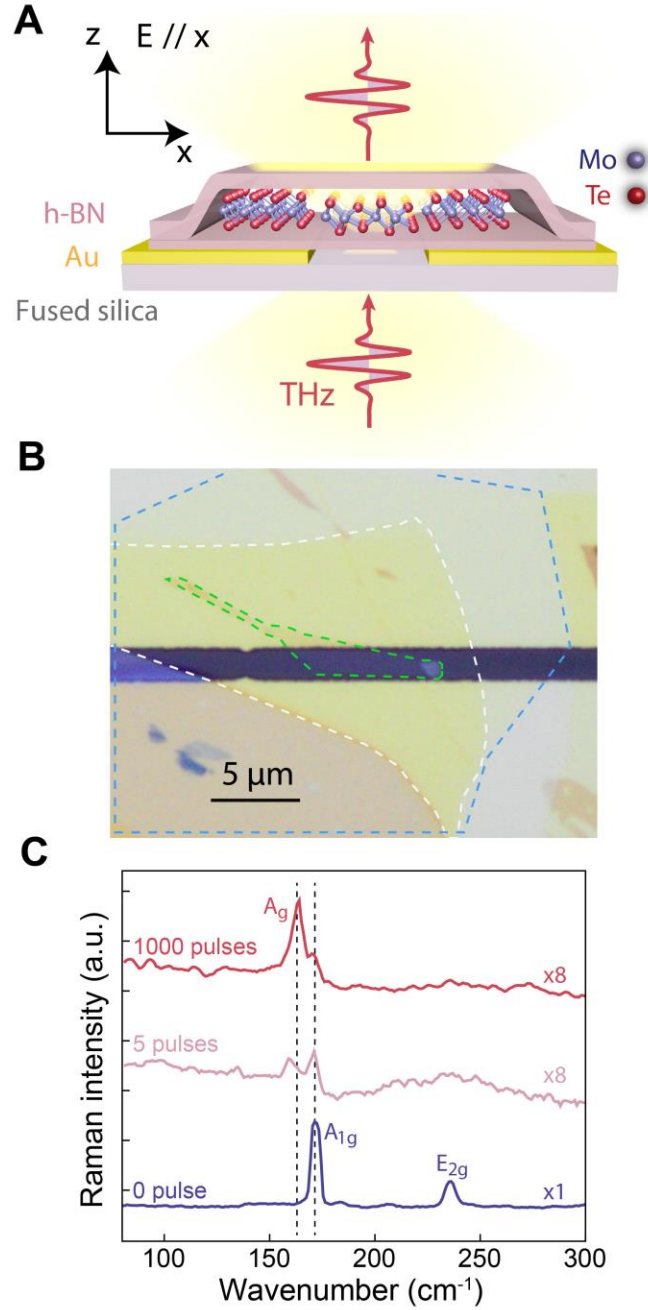


Fig. 2. THz-field-driven metastable topological phase in monolayer MoTe₂. (A) Cross-sectional schematic illustration of a *2H*-MoTe₂ crystal spanning an insulating gap between deposited gold lines, which serves as a THz field enhancement structure. The monolayer *2H*-phase MoTe₂ crystal is encapsulated between top and bottom h-BN. THz pulses are incident from the fused silica substrate side. (B) Optical microscope image of a sample, including 15 nm thick top h-BN (marked by a white dashed line), monolayer *2H*-MoTe₂ (green dashed line), and 5 nm thick bottom h-BN (blue dashed line), all spanning a 1.8- μm insulating gap (dark horizontal line) between gold strips. (C) Raman spectra of monolayer MoTe₂ after successive THz pulse irradiation with free-space field amplitudes of 270 kV/cm. The A_g mode of the *1T'* phase sets in

after 5 THz pulses and dominates upon further THz irradiation; in contrast, the A_{1g} and E_{2g} modes of the $2H$ phase are strongly reduced. The Raman measurements were conducted with a 1 μm diameter laser spot and were therefore averaged over regions that had been subjected to varying enhanced THz field strengths.

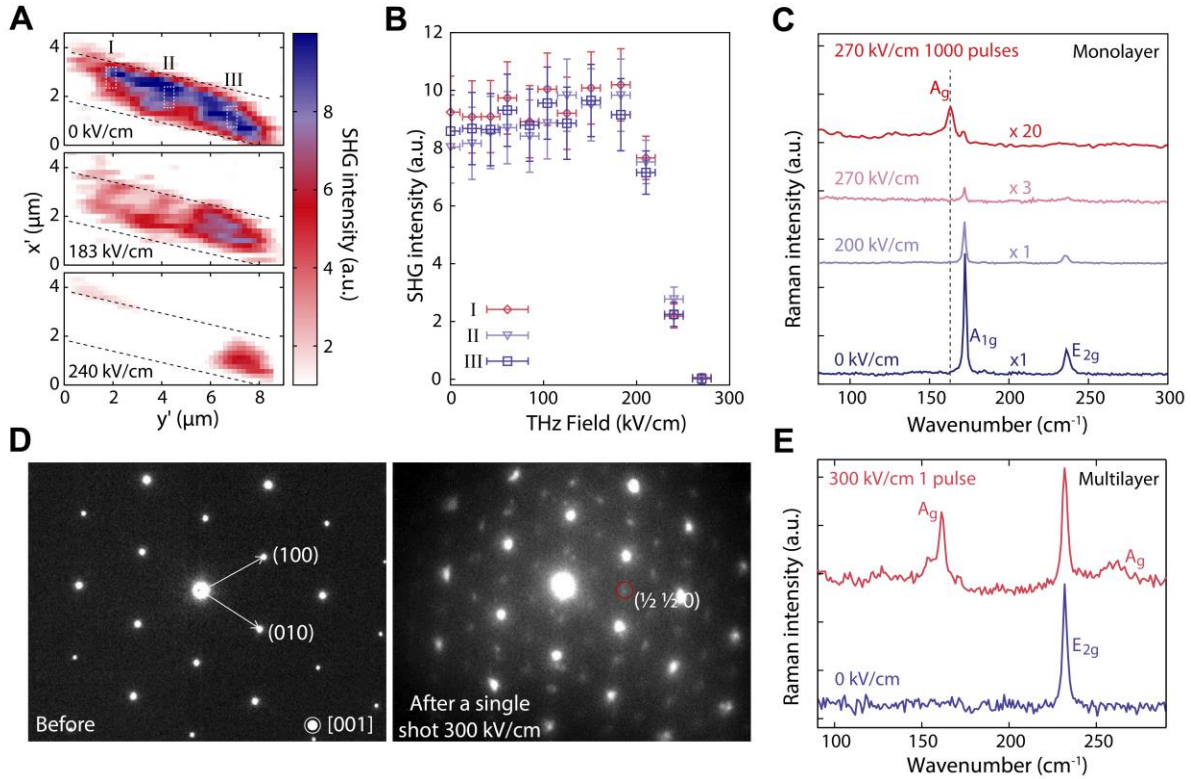


Fig. 3. THz field dependence of the phase transition in monolayer and multilayer MoTe₂. (A) SHG images of monolayer MoTe₂ before THz irradiation (0 kV/cm), after irradiation with a single THz pulse at 183 kV/cm field amplitude, and after irradiation with a second THz pulse at 240 kV/cm. The dashed lines indicate the edges of gold layers in the field enhancement structure. Different areas of monolayer MoTe₂ in the gap are labeled I, II and III. (B) SHG from different spots (I-III) in Fig. 3A measured after irradiation of the sample by single THz pulses with successively increasing field strength. The SHG signal starts to decrease at a free-space field strength of 200 kV/cm and disappears above 240 kV/cm. (C) Raman spectra of monolayer MoTe₂ samples prior to THz irradiation (blue curve), after THz irradiation with a single pulse at 200 kV/cm (violet curve), another single pulse at 270 kV/cm (pink curve), and 1000 pulses at 270 kV/cm (red curve). The Raman modes of the 2H phase start to decrease after a single THz pulse above 200 kV/cm. The monolayer MoTe₂ sample shows the A_g mode at 163.5 cm⁻¹ after irradiation with 1000 pulses at 270 kV/cm. (D) Electron diffraction pattern of multilayer (~10 layers) MoTe₂ before and after a single THz pulse irradiation at 300 kV/cm. Before irradiation, the pattern shows the initial 2H phase characteristics. After a single THz pulse excitation, the electron diffraction shows the features of the induced 1T' phase. (E) Raman spectrum of the multilayer MoTe₂ before and after a single THz pulse irradiation at 300 kV/cm. The emergence of new Raman peaks that are fingerprints of the induced 1T' phase is apparent.

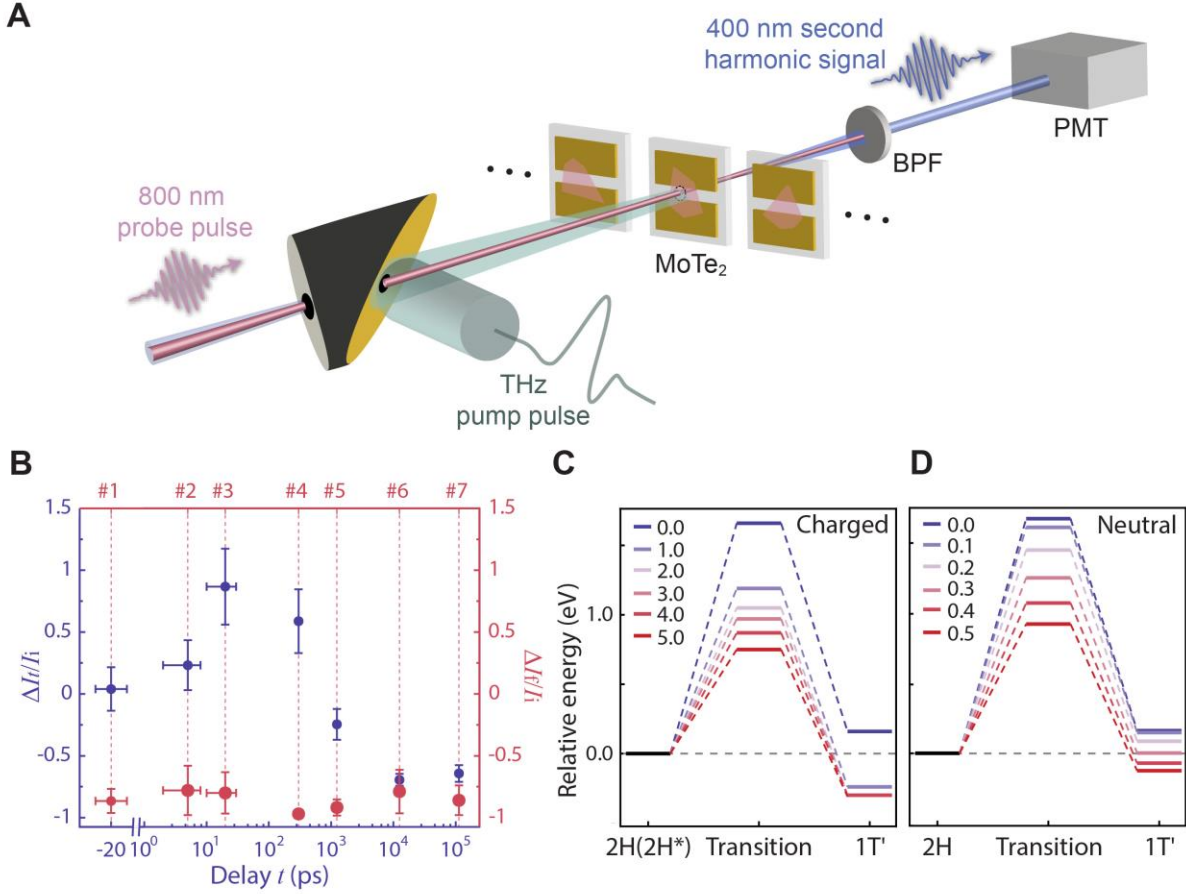


Fig. 4. THz-field-induced topological phase transition dynamics and the driving mechanism. (A) Schematic illustration of single-shot SHG probe with a THz excitation pulse. Single-shot measurements were conducted by replenishing samples in each shot. (B) SHG intensities measured from seven trilayer MoTe₂ samples at different delay times t from several picoseconds to hundreds of nanoseconds (blue dots) as well as around 1 minute (red dots). The data points on the same dashed line show the SHG intensity changes measured from the same sample shortly after (ΔI_i) and long after the THz excitation pulse (ΔI_f), normalized by the SHG signal intensity prior to THz excitation (I_i). The error analysis is provided in Supplementary Note 2. (C) The energy potential as a function of transition coordinate upon charge dopings. As the added charge density increases to 1.0 e/MoTe_2 , which corresponds to $9 \times 10^{14} \text{ cm}^{-2}$, the activation energy decreases from 1.66 to 1.19 eV. The figure legend has a unit of e/MoTe_2 . (D) The energy potential as a function of transition coordinate with nonequilibrium carrier distribution (charge neutral). Nonequilibrium distribution of carriers is qualitatively described by the Fermi-smearing method. The free-energy barrier decreases from 1.66 to 0.91 eV as the Fermi-smearing width increases from 0.0 to 0.5 eV. The figure legend has a unit of eV. The atomic structures of transition states are displayed in Supplementary Figs. S17 and S18.